University of California, Berkeley

Department of Bioengineering

From Lab to Clinic: Automating Nanoparticle Purification and Coating for Magnetic Particle Imaging

MEng Capstone Final Report

Project ID: 113

Team Members

Prithvish Ganguly (BioE), **Lucas Pierce** (MSE), **Shuqing Zhao** (BioE)

Advisor

Professor Steven Conolly

Spring 2026

Contents

List of Figures

I. Executive Summary

Magnetic Particle Imaging (MPI) is an emerging medical imaging modality that detects superparamagnetic iron oxide (SPIO) tracers in real time, with no ionizing radiation and no background tissue signal. Its key differentiator from MRI, CT, and PET is that it produces images in which signal intensity scales linearly with local tracer concentration. In other words, image brightness can be converted directly to a tracer concentration value, rather than to a relative contrast level. This linear, background-free response enables high-contrast, quantitatively interpretable images of tracer distribution.

However, MPI performance is fundamentally limited by variability in nanoparticle magnetic behavior. Conventional synthesis produces heterogeneous particle populations whose mixed magnetic responses broaden the system point spread function (PSF), the imaged response of a single point source. The width of the PSF sets the achievable spatial resolution, and broadening therefore degrades both spatial resolution and signal consistency. Existing approaches that focus on hardware or reconstruction algorithms cannot fully overcome this limitation, making tracer optimization a critical bottleneck for clinical translation.

This project develops a scalable, end-to-end pipeline that improves MPI tracer performance through coordinated nanoparticle purification and stabilization. A geometry-controlled magnetophoretic device, referred to as the MagStick, selectively captures chain-forming superferromagnetic iron oxide nanoparticles (SFMIOs) while leaving non-interacting SPIOs in the supernatant. Following purification, a silica encapsulation process, informally referred to as mochi encapsulation, deposits a uniform shell on each enriched particle, fixing the interparticle spacing of the chains they form, a process referred to as corndogging, at the magnetically optimal distance.

Selection and encapsulation play complementary roles. The MagStick narrows the population to the strongest magnetic responders, while the silica shell preserves the tighter distribution by preventing aggregation, drift, and spacing changes that would otherwise reintroduce variability over time.

Three experiments validate the MagStick across increasing tracer complexity, using the standard MagRack as the benchmark. In Experiment 1, using an SFMIO/SPIO mixture as a proof of concept, MagStick achieved approximately 6.1 mT FWHM at 40 mT applied field versus approximately 11 mT for the standard MagRack, against a 25.7 mT unwashed baseline. In Experiment 2, using an SPIO-only tracer, MagStick achieved approximately 3.3 mT FWHM at 5 mT, compared with approximately 3.6 mT for the MagRack. In Experiment 3,

using an SFMIO-only tracer with a parameter sweep over dilution and dip time, the best condition, a 1:5 dilution in chloroform with a single 15-minute dip, produced 1.5 mT FWHM at 10 mT applied field, approaching the MagRack reference of approximately 1.0 mT, but in one passive wash rather than three MagRack resuspension cycles.

Overall, this work contributes a tracer-engineering pathway that complements ongoing hardware and reconstruction efforts in MPI. Rather than replacing those approaches, it removes an upstream limit on what they can achieve. Future work will focus on automating the purification process, improving coating uniformity through controlled chemistry, and validating tracer performance in biological and pre-clinical environments.

II. Context and Background

II.A. Introduction: Problem Context and Motivation

Magnetic Particle Imaging has emerged as a promising imaging modality because it directly detects magnetic nanoparticle tracers and produces images whose pixel intensities map linearly to local tracer concentration. Combined with the absence of any background signal from tissue, this property positions MPI as a candidate technology for vascular imaging, cell tracking, gastrointestinal bleed detection, cancer imaging, and theranostic applications.

Despite advances in scanner design and image reconstruction, MPI performance is fundamentally constrained by tracer behavior. In this context, tracer behavior refers to the physical properties of the nanoparticles themselves, including magnetic moment, relaxation dynamics, saturation behavior, interparticle coupling, and aggregation state. These factors determine the shape of the magnetization response curve, which directly affects both signal strength and spatial resolution.

The central challenge is the heterogeneity of nanoparticle populations produced through conventional synthesis. Variations in particle size, magnetic moment, and relaxation behavior broaden the PSF and reduce spatial resolution. Prior work has shown that collective magnetic interactions and particle coupling effects play a critical role in determining MPI performance, and that engineered nanoparticle systems can achieve substantial gains in resolution and sensitivity when these interactions are properly controlled [1]. These findings indicate that optimizing nanoparticle properties is essential for advancing MPI.

One promising approach is magnetophoretic separation, which uses magnetic field gradients to isolate particles based on magnetic response rather than size alone. This enables enrichment of high-performance subpopulations. Both theoretical and experimental studies have characterized how interparticle interactions, chaining effects, and field geometry affect separation efficiency and selectivity [2, 3, 4]. Separation alone, however, is not sufficient. Isolated nanoparticles may still drift over time as aggregation and changes in interparticle spacing alter their effective magnetic behavior. Post-synthesis stabilization strategies such as silica encapsulation have therefore been explored to control particle spacing and modulate magnetic interactions [5, 6]. Together, these observations motivate a coordinated strategy that combines selection with stabilization.

II.B. Background: Existing Approaches and Limitations

Existing efforts to improve MPI performance fall into three primary domains: hardware optimization, computational reconstruction, and nanoparticle engineering. Each has contributed incremental gains, but none individually resolves the underlying problem of tracer heterogeneity.

Hardware-based strategies focus on increasing magnetic field gradients and improving scanner sensitivity to enhance spatial resolution. While these advances yield real improvements, they introduce additional system complexity and cost without directly addressing variability in tracer behavior [7, 8]. Reconstruction-based strategies can partially compensate for signal dispersion through model-based and learned image reconstruction, but no algorithm can eliminate intrinsic variability in nanoparticle magnetic response [9, 10].

As a result, nanoparticle engineering has emerged as a primary focus for improving MPI performance. Prior studies have demonstrated that collective magnetic behavior, particularly superferromagnetism, can significantly enhance imaging resolution and sensitivity by promoting coordinated particle interactions [1, 11]. Surface engineering techniques have also been used to tune interparticle spacing and magnetic coupling. Silica coating, for example, can regulate nanoparticle interactions and influence magnetic relaxation, with shell thickness acting as a key design parameter [5, 6].

Despite these advances, synthesis-based approaches face an inherent limit. Even highly controlled fabrication produces a distribution of particle properties, and post-synthesis heterogeneity remains unavoidable. This reduces reproducibility across batches and limits tracer consistency.

Post-synthesis purification strategies have therefore been explored to refine nanoparticle populations after fabrication. Traditional techniques such as centrifugation and chromatographic separation can narrow hydrodynamic size distributions, but they do not directly select for the magnetic-response characteristics that matter most for MPI. This creates a need for magnetic-response-based purification methods.

II.C. Magnetophoresis: Implementation Gap and Opportunity

Magnetophoresis is the motion of magnetic particles under an applied magnetic field gradient. In simplified form, the magnetic force acting on a particle can be expressed as

$$F_m = m\mu_0 \nabla H, \tag{1}$$

where m is the magnetic moment of the particle, μ_0 is the magnetic permeability of free space, and ∇H is the magnetic field gradient. This force is resisted by viscous drag. For a spherical particle in low-Reynolds-number flow, the drag force is

$$F_d = 6\pi\eta R v, \tag{2}$$

where η is the fluid viscosity, R is the particle radius, and v is the particle velocity.

At steady state, magnetic force and drag balance, so particles with larger magnetic moments migrate faster under the same gradient. This provides the physical basis for magnetic-response-based separation.

Theoretical models predict that particles with stronger magnetic responses can be preferentially separated under appropriate field conditions [2, 4]. Experimental work has also confirmed that magnetophoretic separation can enrich nanoparticle populations and improve MPI tracer performance [3]. Studies of particle chaining and cooperative dynamics further show that separation efficiency depends not only on individual particle properties but also on collective effects within the suspension [12].

In practice, however, two implementation paradigms dominate, and each has clear shortcomings. Bulk separation methods that use permanent magnets in tubes or beakers are simple and high-throughput, but they lack spatial control. Particles near the magnet experience much larger forces than particles farther away, so the selected population is shaped partly by particle starting position rather than by magnetic response alone [13]. Microfluidic systems take the opposite trade-off. By constraining flow and field gradients, they achieve precise, well-characterized selection, but their channel geometries, fabrication requirements, and low volumetric throughput make them difficult to scale [14].

The result is an open gap between highly controlled but low-throughput devices and scalable but imprecise methods. The MagStick is designed to operate in that gap.

II.D. Integrated Strategy: Selection and Stabilization

Neither synthesis nor purification alone is sufficient to produce consistent, high-performance MPI tracers. Magnetophoretic separation can selectively enrich nanoparticles with desirable magnetic properties, but it does not address post-selection stability. Aggregation and drift

in interparticle spacing can erode the very improvements that selection achieved.

Conversely, surface engineering techniques such as silica coating can stabilize behavior over time, but they cannot eliminate the underlying heterogeneity of the starting population. The two approaches are therefore complementary. This project pairs them so that selection narrows the population while stabilization preserves the result.

II.E. Project Positioning and Contribution

This project builds on prior work in magnetophoretic separation and nanoparticle surface engineering by integrating the two into a single, scalable refinement pipeline. The MagStick contributes a geometry-controlled purification stage that improves selection consistency by constraining particle–magnet distance. This is coupled with silica-based stabilization that aims to lock in the optimized behavior obtained from selection.

By targeting both selection and stability within a single workflow, the approach addresses limitations identified in prior methods and offers a practical pathway toward more reproducible MPI tracers.

III. Technical Approach and Outcomes

III.A. System Overview: Integrated Tracer Optimization Pipeline

The project implements an integrated tracer optimization pipeline with two coordinated stages. The first stage is magnetophoretic purification using the MagStick, which selectively enriches nanoparticles with strong magnetic responses. The second stage is silica encapsulation, which stabilizes that enriched population by controlling interparticle spacing and preventing aggregation that would otherwise re-introduce variability.

The two stages are designed as a continuous workflow rather than as independent processing steps. Purification defines the desired particle population, and stabilization preserves its optimized behavior, so that the gains achieved in selection remain present after storage and handling.

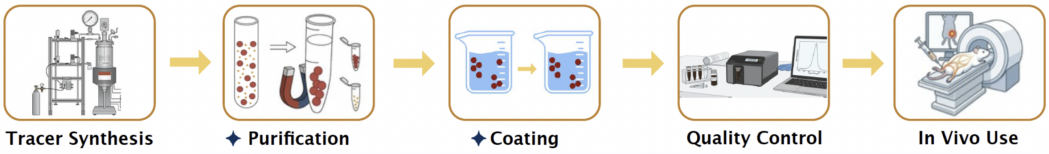

Figure 1: Overview of the MPI tracer synthesis and optimization pipeline, highlighting the integration of magnetophoretic purification and silica encapsulation stages within the broader tracer development process.

III.B. Magnetophoretic Purification System: MagStick

Magnetophoretic purification selects nanoparticles based on their magnetic response rather than their size or mass alone. In a magnetic field gradient, each nanoparticle experiences a force proportional to its magnetic moment and to the local gradient of the field. This force competes with hydrodynamic drag, so chain-forming SFMIOs with stronger magnetic responses can be preferentially captured under controlled conditions while weaker responders remain in suspension.

The MagStick is designed to provide the geometric control of a microfluidic device without requiring channel fabrication or active flow control. At the same time, it retains the simplicity of a bulk separation method without inheriting the non-uniform field exposure associated with placing a magnet outside a tube.

The MagStick is a thin cylindrical assembly designed to insert directly into a 15 mL Corning tube containing the tracer suspension. It comprises three main components:

(i) a thin cylindrical mesh outer shell that allows tracer access while protecting the magnet array from direct contact with chain-forming particles;

(ii) a central inner core rod housing the magnet array;

(iii) a stack of 1/8-inch NdFeB cylindrical magnets that generates the local magnetic field gradient.

The shell-to-core clearance is approximately 0.5 mm. This displaces the tracer into a narrow annular volume close to the magnets and shortens the effective particle–magnet distance. A purpose-built MagStick holder positions the device at an angle in the tube, preventing the captured SFMIO fraction from pooling at the bottom and instead distributing it along the length of the magnet stack.

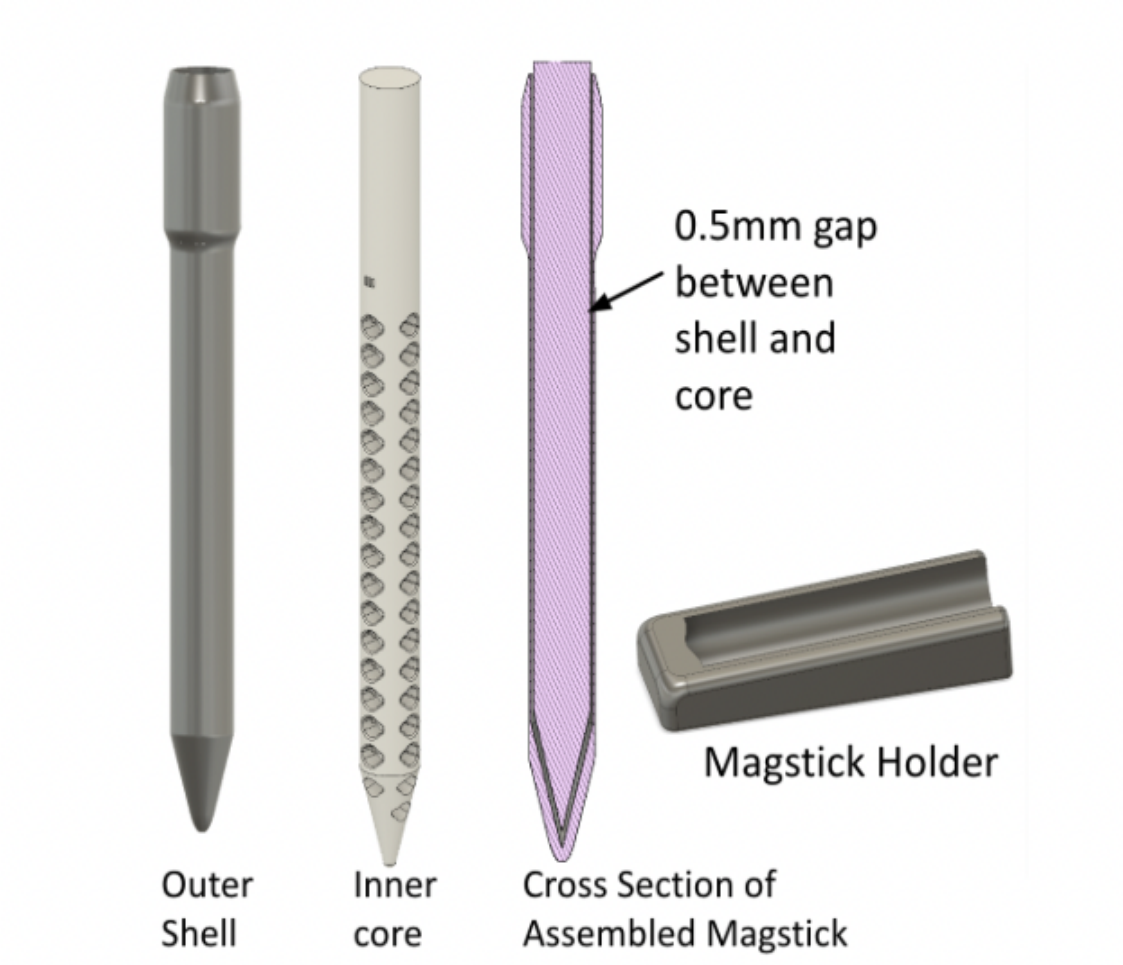

Figure 2: Geometry-controlled MagStick device for magnetophoretic purification. A 0.5 mm gap between the outer shell and inner core regulates particle–magnet distance, enabling more uniform magnetic field exposure and consistent selection conditions.

The purification workflow proceeds in four stages:

1. **Sample loading:** A heterogeneous nanoparticle suspension is added to the tube.
2. **Magnetic capture:** Nanoparticles with higher magnetic moments migrate toward the MagStick under the imposed field gradient, while lower-response particles remain in suspension.
3. **Transfer and wash:** The MagStick is moved into a clean wash solution, displacing loosely or non-specifically bound particles and improving selection purity.
4. **Magnetic release:** The field is removed, allowing the captured high-response population to detach into a clean collection medium.

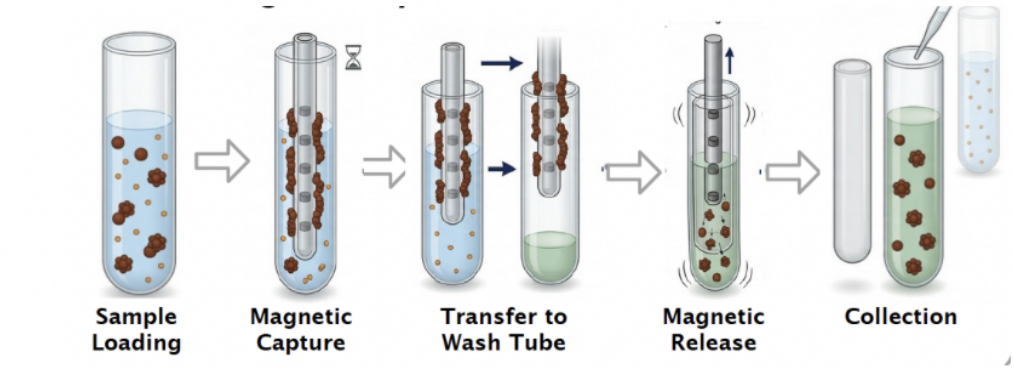

Figure 3: Geometry-controlled magnetophoretic purification process using the MagStick, illustrating selective capture, transfer, and enrichment of high-magnetic-response nanoparticles under controlled field exposure.

Two practical advantages follow from this geometry. First, the narrowed distribution of particle–magnet distances yields more consistent selection outcomes from run to run, because the selection threshold is set primarily by particle properties rather than by where particles happen to sit relative to the magnet. Second, the device scales by parallelization rather than by device redesign. Because each MagStick is a self-contained probe operating in a standard 15 mL tube, throughput can be increased by running multiple sticks in parallel on a rack.

III.C. Silica Encapsulation and Stabilization Strategy

Silica encapsulation, informally referred to as mochi encapsulation, performs two functions. First, it sets a fixed geometric spacing between adjacent particles in the chains they naturally form under field. This spacing directly tunes magnetic strength and coercivity, where coercivity refers to the field required to flip the internal magnetization.

When particles are too far apart, their fields reinforce each other less, lowering the chain's effective magnetic strength. When particles are too close, the coercive field rises. A controlled center-to-center spacing is therefore needed to balance these two effects. Second, depositing a uniform shell of the same thickness on every selected particle homogenizes this spacing across the population, so that the magnetic properties selected by the MagStick are not later eroded by uneven interparticle distances.

The chemistry follows an established silica-coated nanoparticle route. Tetraethyl orthosilicate (TEOS) acts as the silicon source. It hydrolyzes and condenses on the nanoparticle surface to form a silica shell. Ammonia catalyzes hydrolysis, and the surfactant Igepal

CO-520 forms inverse micelles that confine the reaction near each nanoparticle, promoting heterogeneous nucleation on the particle surface rather than homogeneous nucleation in bulk solution.

The relative concentrations of TEOS, ammonia, and Igepal control whether the reaction yields well-coated nanoparticles or off-target byproducts. Excess ammonia can generate too much intermediate $Si(OH)_4$, which self-nucleates into free silica microspheres rather than depositing on the nanoparticle surface. Excess Igepal can provide additional micellar surface area for TEOS to nucleate on. Excess TEOS can lead to agglomeration as adjacent shells grow into one another. The chemistry therefore exists inside a concentration window, and the experimental work focuses on locating that window.

III.D. Experimental Methods and Evaluation Metrics

The pipeline was evaluated by running tracer samples through one or both stages and measuring imaging-relevant properties before and after processing. The standard MagRack, a permanent-magnet rack operated at Eppendorf scale with the captured pellet repeatedly resuspended through wash cycles, served as the benchmark for purification performance.

Three experiments were run with increasing tracer complexity:

1. a fabricated SFMIO/SPIO mixture as a proof-of-concept tracer;
2. a single-core SPIO-only tracer as an intermediate validation step;
3. an SFMIO-only tracer with a parameter sweep over dilution ratio and dip time.

A separate PTFE coating validation experiment characterized the chloroform resistance of the MagStick shell.

The primary evaluation metric was PSF FWHM, measured on an MPI relaxometer. A narrower PSF corresponds to higher spatial resolution, and FWHM is a standard scalar summary of PSF width in MPI. Reproducibility was assessed by comparing FWHM values across repeated runs of the same condition. Throughput was reported as microliters of source tracer processed per run. Qualitative indicators, including aggregation tendency and visual uniformity in TEM images, were tracked alongside the quantitative metrics.

III.E. Results and Performance Analysis

III.E.1. MagStick Fabrication

The MagStick outer shell was 3D printed in Clear V4 SLA resin on a Form 3 printer at a 0.025 mm tolerance. It was sized to fit a 15 mL Corning tube with a 0.5 mm gap that promotes upward displacement of the tracer into contact with the embedded magnets.

Because the tracer is suspended in chloroform, a dry-film PTFE coating process was developed using repeated coat–dry–bake cycles at 110 °C. Uncoated shells degraded within approximately two hours of chloroform exposure, while PTFE-coated shells remained intact across all observed timepoints and were reused across multiple purification runs without observable degradation.

III.E.2. Experiment 1: SFMIO/SPIO Mixture

Experiment 1 used a fabricated mixture of multicore SFMIOs and single-core SPIOs as a clean proof-of-concept tracer. The pre-MagStick unwashed baseline was 25.7 mT FWHM at 40 mT and 20 kHz. MagStick achieved approximately 6.1 mT FWHM at 40 mT applied field, compared with approximately 11 mT for MagRack. At 10 mT, MagStick achieved approximately 16.5 mT, compared with approximately 17 mT or higher for MagRack. A coercive threshold at approximately 8 mT in the MagStick output confirmed SFMIO enrichment and rejection of non-interacting SPIOs.

III.E.3. Experiment 2: SPIO-Only Tracer

Experiment 2 tested a single-core SPIO-only tracer as an intermediate validation step. The purpose was to confirm that the chloroform workflow and PTFE-coated shell functioned correctly during a real run. MagStick achieved approximately 3.3 mT FWHM at 5 mT applied field, compared with approximately 3.6 mT for MagRack. This demonstrated comparable PSF narrowing at substantially higher per-run volume, but it was an equivalence result rather than a differentiating advantage because SPIOs do not form the chains that MagStick is specifically designed to capture.

III.E.4. Experiment 3: SFMIO-Only Tracer

Experiment 3 was the main validation experiment. It processed an SFMIO-only tracer batch in chloroform using 1 mL per run. Two dilution ratios, 1:9 and 1:5, and three dip conditions, 5 minutes, 15 minutes, and 15 + 15 minutes, were tested on the AWR relaxometer at 10 mT applied field.

The best operating point was a 1:5 dilution with a single 15-minute dip. This produced 1.5 mT FWHM at 10 mT, approaching the MagRack reference of approximately 1.0 mT, which was achieved with three sequential resuspension cycles. MagStick therefore came within approximately 0.5 mT of MagRack performance in a single passive wash, while preserving chain structure and processing approximately 166 µL of source tracer per run versus approximately 40 µL to 50 µL for MagRack.

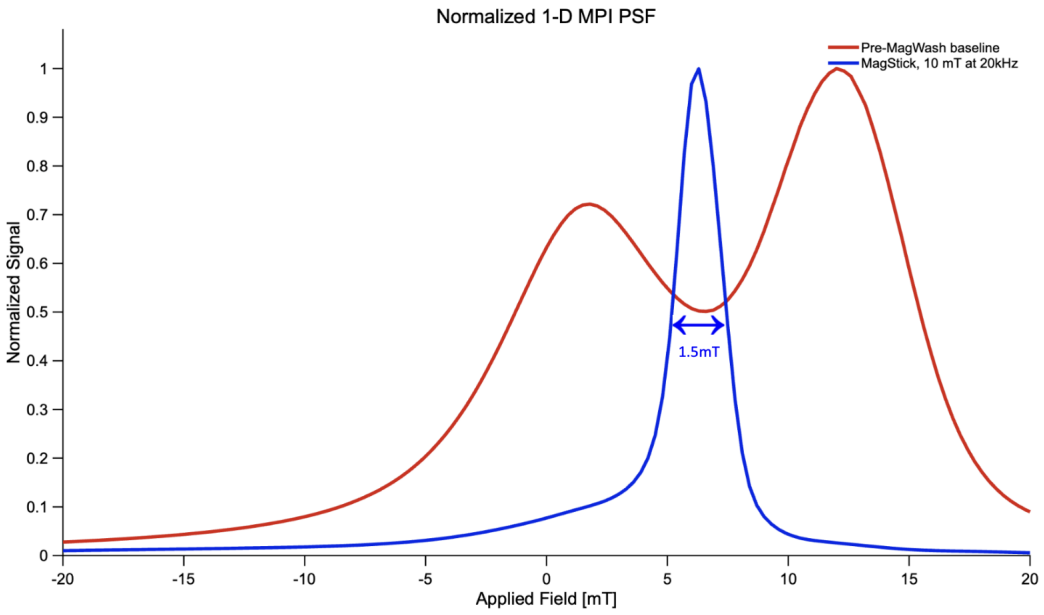

Figure 4: Experiment 3 validation of MagStick using SFMIO tracer under a 10 mT field. The optimal condition, 1:5 dilution with a 15-minute dip, achieved 1.5 mT FWHM, within approximately 0.5 mT of MagRack performance but with a single passive wash and higher throughput.

III.E.5. Silica Encapsulation Results

The success of each encapsulation run was assessed by transmission electron microscopy (TEM), which was used to estimate shell thickness, identify nanoparticle aggregation, and

detect free silica microspheres.

In the first round of experiments, two issues dominated. First, free silica microspheres of approximately 50 nm to 70 nm diameter formed in large numbers throughout the sample, indicating that most of the silica was nucleating in solution rather than depositing on the nanoparticles. This is undesirable because free microspheres consume reagents and are difficult to separate from coated particles afterward.

Second, the nanoparticles themselves aggregated into clumps that prevented uniform silica deposition. On the positive side, the silica shells that did form around individual particles, as well as the free microspheres themselves, were uniform in size and shape and showed no signs of shell–shell agglomeration.

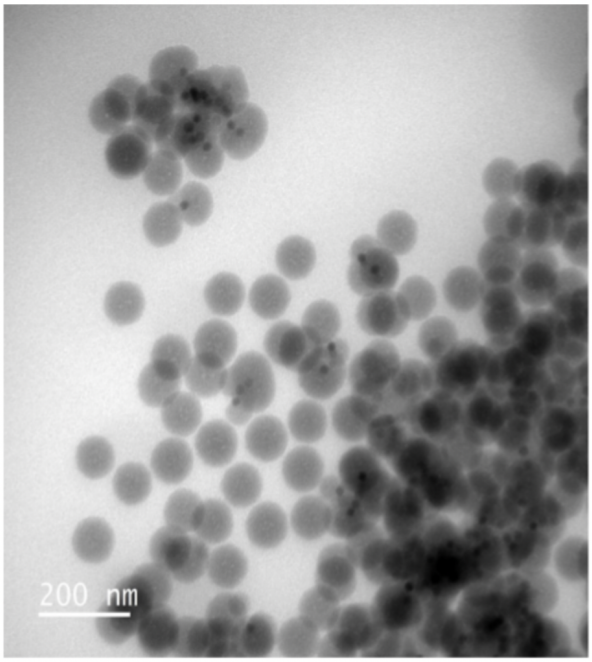

Figure 5: TEM image from the first round of silica encapsulation. Dark dots represent nanoparticles, while the semitranslucent material represents silica. Free silica microsphere formation and nanoparticle aggregation indicate that further chemistry optimization is required.

Two follow-up experimental directions are planned to address these issues. The first is a sweep of the ammonia-to-TEOS ratio to suppress free $Si(OH)_4$ generation and shift nucleation from bulk solution onto the particle surface. The second is sonication of the particle suspension before and between fractionalized TEOS additions, to break up aggregates and expose fresh particle surface for coating. These changes are proposed rather than demon-

strated because results from these experiments are not yet available.

III.F. Discussion and Limitations

MagStick demonstrates reliable PSF narrowing across all three tracer types tested, with the strongest result on the SFMIO-only tracer where chain preservation matters most. A result of 1.5 mT FWHM at 10 mT in a single 15-minute passive wash, compared with a 1.0 mT MagRack reference obtained with three resuspension cycles, supports the feasibility of geometry-controlled passive purification.

The hands-free workflow eliminates the operator-dependent resuspension steps that drive much of MagRack's run-to-run variability. The per-run volume advantage also addresses MagRack's most cited bottleneck. Together, the three experiments address the primary design axes of resolution quality, operational reliability, and processing throughput.

On resolution quality, MagStick matched or approached MagRack performance across all tested conditions. Experiment 3 is the most directly relevant benchmark because it enriches a realistic SFMIO batch to within approximately 0.5 mT of MagRack in a single passive wash cycle. Experiment 1 demonstrated selective retention of chain-forming particles, but it reflects a structurally idealized separation between morphologically distinct particle classes rather than the subtler discrimination expected in a real crude batch. Experiment 2 approached the intrinsic resolution ceiling for a monodisperse SPIO population, where further PSF narrowing is bounded by single-particle magnetic properties rather than separation geometry.

On reliability, the passive dip-and-withdraw mechanism is a structural departure from the operator-sensitive MagRack protocol. In MagRack purification, resuspension force, pipetting consistency, and dwell time vary between users and between runs in ways that are difficult to standardize. MagStick reduces the protocol to insertion, a fixed dip interval, and withdrawal, eliminating active mechanical input during separation. Quantitative inter-operator and inter-run reproducibility were not formally characterized in this study and represent priorities for future validation.

On throughput, each crude synthesis cycle yields approximately 10 mL of tracer. The standard MagRack protocol processes approximately 40 µL to 80 µL per cycle at 10–15 minutes per cycle. Processing a full batch would therefore require many sequential washes and substantial operator time. MagStick, validated at 1 mL per run, reduces this substantially. The 15 mL vessel geometry may support larger fluid volumes while maintaining contact

along the full magnetic shaft, but this was not fully validated experimentally due to tracer conservation constraints.

Several limitations remain. Extraction efficiency was not quantified in absolute terms because no pre-purification particle enumeration was performed. A fraction of captured SFMIOs may be lost during withdrawal, and yield as a function of dip time, dilution ratio, and withdrawal protocol remains to be characterized. The SFMIO-only validation was confined to a single batch, and an anomalous SPIO-like PSF signature observed in an earlier SFMIO run remains mechanistically unresolved. Device-level variability arising from magnet-to-magnet repulsion during embedding and partial chain disruption on withdrawal should also be addressed in subsequent design iterations. Finally, the silica encapsulation chemistry remains partially validated; ammonia/TEOS ratio optimization and sonication protocols are pending experimental completion.

IV. Implications and Future Work

IV.A. Implications

These results support the broader argument that controlling nanoparticle populations at the ensemble level is a productive lever for MPI optimization. This approach should be understood as complementary to, not in place of, ongoing work on hardware and reconstruction. The literature already identifies tracer heterogeneity as a major constraint on current MPI performance, and this project contributes a concrete processing method for reducing it.

Hardware and reconstruction strategies remain necessary. Better field gradients improve the ceiling on what any tracer can deliver, and improved reconstruction algorithms continue to extract more information from a given measurement. The point of this work is complementary: those gains are bounded above by the variability of the underlying particle population, and reducing that variability raises the ceiling for the entire imaging pipeline.

The integration of silica encapsulation adds a stabilization step that aims to help the optimized behavior persist. By controlling interparticle spacing and limiting aggregation, the coating process is intended to keep selected populations consistent across samples and over time. Because the encapsulation chemistry is not yet fully tuned, this is currently a framework supported by partial experimental evidence rather than a fully demonstrated end-to-end result.

Taken together, the findings suggest that coordinated nanoparticle refinement, combining

selection and stabilization, is a useful additional axis along which MPI tracer performance can be optimized.

IV.B. Future Work

While the proposed pipeline shows improvements in tracer performance, additional work is needed to realize its scalability and practical implementation.

One direction is to improve the geometric and microfluidic precision of the magnetophoretic stage. This would help maintain uniform field exposure across larger sample volumes and higher flow conditions. A second direction is automation of the purification process. Replacing manual insertion and withdrawal with a controlled actuator and integrating field-positioning control would reduce user-dependent variability and enable higher-throughput operation.

In parallel, optimization of the silica encapsulation chemistry is needed to achieve consistent shell thickness and uniform coating across the particle population. This includes the ammonia/TEOS sweep and sonication protocol described earlier. Looking further ahead, integrating purification and stabilization with upstream nanoparticle synthesis would create a continuous, scalable production pipeline.

Validation in fully developed MPI systems and biologically relevant environments will be essential for assessing clinical applicability and confirming that improvements observed in benchtop experiments translate to in vivo conditions.

V. Conclusion

MPI performance is currently constrained by nanoparticle heterogeneity, which limits spatial resolution and signal consistency in ways that hardware and reconstruction advances alone cannot fully resolve. This project addresses that constraint through a coordinated tracer-engineering strategy that integrates geometry-controlled magnetophoretic purification with post-selection stabilization.

The dipstick-based MagStick system uses constrained particle–magnet geometry to enforce more uniform field exposure than conventional bulk methods provide. It selectively enriches nanoparticles with favorable magnetic responses, while subsequent silica encapsulation and controlled chain formation are intended to lock in interparticle spacing and preserve optimized behavior over time.

Experimental results support the effectiveness of the purification stage. On the fabricated SFMIO/SPIO mixture, MagStick achieved approximately 6.1 mT FWHM at 40 mT applied field, compared with approximately 11 mT for standard MagRack. On a single-core SPIO tracer, MagStick produced approximately 3.3 mT FWHM at 5 mT, comparable to MagRack. On the SFMIO-only tracer, the best condition achieved 1.5 mT FWHM at 10 mT, approaching the MagRack reference while using a single passive wash.

The silica encapsulation stage is partially validated. Shell formation around individual particles was confirmed, but suppression of free silica microspheres and aggregation requires further chemistry optimization.

Beyond the specific implementation, this work contributes a framework for MPI tracer optimization based on coordinated, pipeline-level design. Selection and surface engineering are treated as a coupled process rather than as independent steps, making nanoparticle behavior more predictable and tunable in practice.

In summary, combining geometry-controlled purification with controlled stabilization is an effective and scalable way to address current limits on MPI tracer quality. By reducing nanoparticle heterogeneity and improving reproducibility, the approach supports the broader effort to translate MPI into reliable clinical and industrial use.

References

[1] Zhi Wei Tay et al. "Superferromagnetic nanoparticles enable order-of-magnitude resolution and sensitivity gain in magnetic particle imaging". In: *Small Methods* 5.11 (Nov. 2021), e2100796. DOI: 10.1002/smtd.202100796. URL: https://doi.org/10.1002/smtd.202100796.

[2] J. S. Andreu et al. "Simple analytical model of magnetophoresis in a magnetic field gradient". In: *Physical Review E* 84 (2011), p. 021402. DOI: 10.1103/PhysRevE.84.021402. URL: https://journals.aps.org/pre/abstract/10.1103/PhysRevE.84.021402.

[3] Soudabeh Arsalani et al. "Magnetic separation of iron oxide nanoparticles to improve their application for magnetic particle imaging". In: *Physics in Medicine and Biology* 66.1 (Jan. 2021), p. 015002. DOI: 10.1088/1361-6560/abcd19. URL: https://doi.org/10.1088/1361-6560/abcd19.

[4] S. S. Leong et al. "Unified view of magnetic nanoparticle separation under magnetophoresis". In: *Langmuir* 36.28 (June 2020), pp. 8033–8055. DOI: 10.1021/acs.langmuir.0c00839. URL: https://doi.org/10.1021/acs.langmuir.0c00839.

[5] S. L. Pinho et al. "Fine tuning of the relaxometry of gamma-Fe2O3@SiO2 nanoparticles by tweaking the silica coating thickness". In: *ACS Nano* 4.9 (2010), pp. 5339–5349. DOI: 10.1021/nn101129r. URL: https://doi.org/10.1021/nn101129r.

[6] H. L. Ding et al. "Fe3O4@SiO2 core/shell nanoparticles: The silica coating regulations with a single core for different core sizes and shell thicknesses". In: *Chemistry of Materials* 24.23 (2012), pp. 4572–4580. DOI: 10.1021/cm302828d. URL: https://doi.org/10.1021/cm302828d.

[7] T. M. Buzug et al. "Magnetic particle imaging: introduction to imaging and hardware realization". In: *Zeitschrift für Medizinische Physik* 22.4 (Dec. 2012), pp. 323–334. DOI: 10.1016/j.zemedi.2012.07.004. URL: https://pubmed.ncbi.nlm.nih.gov/22909418/.

[8] M. Erbe, T. F. Sattel, and T. M. Buzug. "Improved field free line magnetic particle imaging using saddle coils". In: *Biomedical Engineering / Biomedizinische Technik* 58.6 (Dec. 2013), pp. 577–582. DOI: 10.1515/bmt-2013-0030. URL: https://pubmed.ncbi.nlm.nih.gov/23934634/.

[9] F. Mohn et al. "System matrix based reconstruction for pulsed sequences in magnetic particle imaging". In: *IEEE Transactions on Medical Imaging* 41.7 (July 2022), pp. 1862–1873. DOI: 10.1109/TMI.2022.3149583.

[10] J. Zhao et al. "MPIGAN: An end-to-end deep based generative framework for high-resolution magnetic particle imaging reconstruction". In: *Medical Physics* 51.8 (Aug. 2024), pp. 5492–5509. DOI: 10.1002/mp.17104. URL: https://pubmed.ncbi.nlm.nih.gov/38700948/.

[11] C. Saayujya et al. "Physicochemical necessary and sufficient conditions for superferromagnetism in high-resolution magnetic particle imaging". In: *Small* 21.44 (Nov. 2025), e04794. DOI: 10.1002/smll.202504794. URL: https://doi.org/10.1002/smll.202504794.

[12] S. Ota and Y. Takemura. "Characterization of Néel and Brownian relaxations isolated from complex dynamics influenced by dipole interactions in magnetic nanoparticles". In: *Journal of Physical Chemistry C* 123.47 (2019), pp. 28712–28720. DOI: 10.1021/acs.jpcc.9b06790. URL: https://pubs.acs.org/doi/10.1021/acs.jpcc.9b06790.

[13] X. Wu et al. "SPIONs Magnetophoresis and Separation via Permanent Magnets: Biomedical and Environmental Applications". In: *Processes* 11.12 (Nov. 2023), p. 3316. DOI: 10.3390/pr11123316. URL: https://doi.org/10.3390/pr11123316.

[14] L. Zeng et al. "High-Resolution Separation of Nanoparticles Using a Negative Magnetophoretic Microfluidic System". In: *Micromachines* 13.3 (Feb. 2022), p. 377. DOI: 10.3390/mi13030377. URL: https://doi.org/10.3390/mi13030377.

A. Appendices

A.1. Supplementary Figures

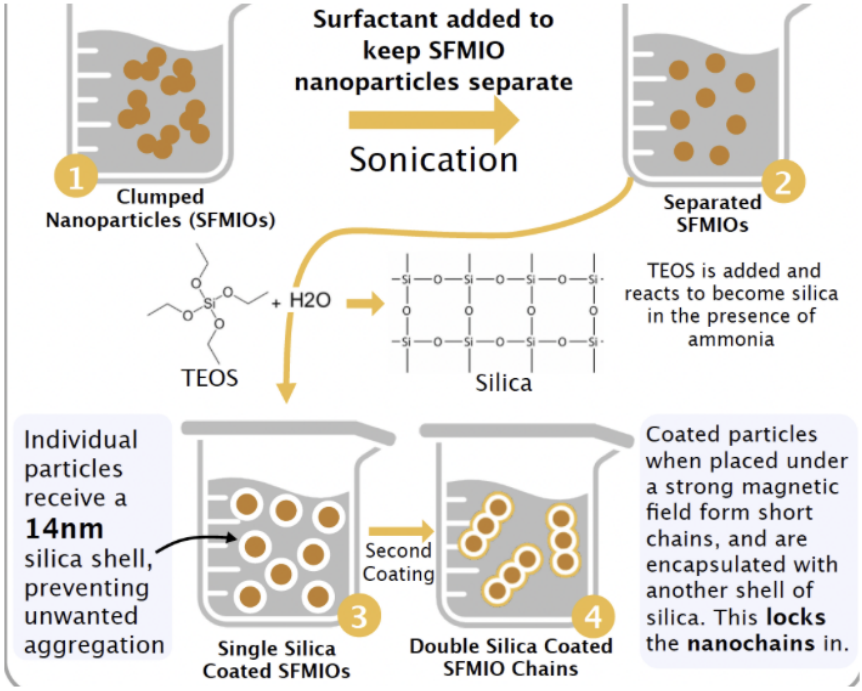

Figure 6: Supplementary characterization data for the MagStick purification workflow.

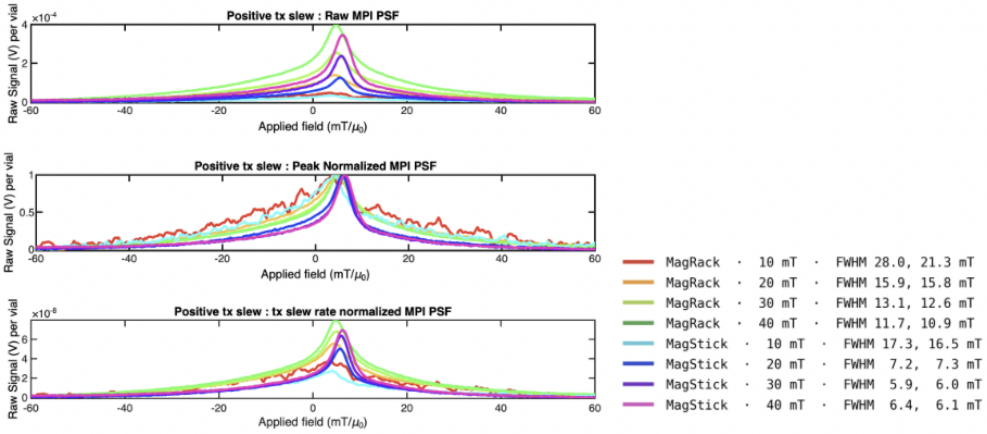

Figure 7: Experiment 1 supplementary results comparing MagStick and MagRack purification using the fabricated SFMIO/SPIO mixture.

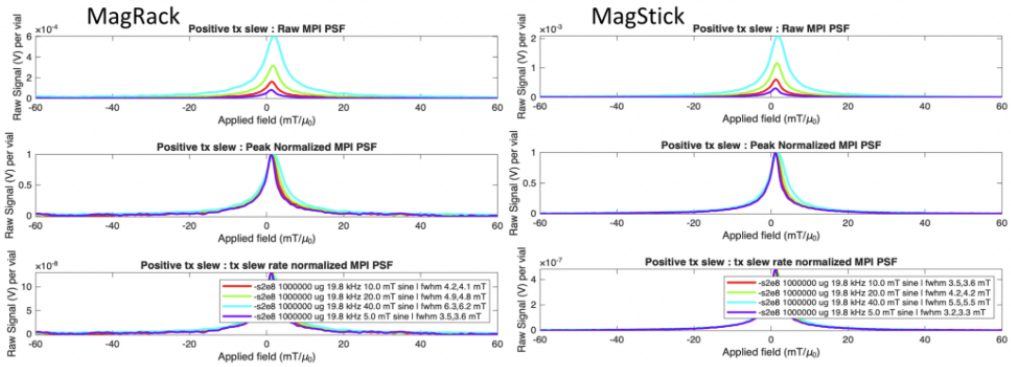

Figure 8: Experiment 2 supplementary results validating the MagStick workflow using the SPIO-only tracer.

A.2. Supplementary Table

Axis	MagStick result	MagRack benchmark	Verdict
Quality (PSF FWHM)	Best 1.5 mT @ 10 mT (Exp 3, SFMIO); ~3.3 mT @ 5 mT (Exp 2, SPIO); ~6.1 mT @ 40 mT (Exp 1, mixture)	~1.0 mT @ 10 mT (SFMIO, 3 cycles); ~3.6 mT @ 5 mT (SPIO); ~11 mT @ 40 mT (mixture)	Comparable on SPIO and mixture; approaches MagRack on SFMIO-only; protocol tuning may close remaining gap.
Throughput (per run)	~166 µL tracer at 1:5 dilution; theoretical headroom up to ~3000 µL per stick (tube-volume limited)	~40–50 µL per Eppendorf-scale wash cycle (and 3–5 cycles per purification)	3–4× higher per single MagStick. Extraction efficiency not yet quantified; some SFMIOs may be left behind.
Reliability (workflow)	Single passive "set-and-leave" dip; insert, wait, withdraw, single transfer	3–5 manual resuspend cycles per purification; operator-dependent; chain disruption on resuspension	Promising. Lower operator variability and chain-preserving by design; more runs needed for statistical confidence.

Figure 9: Supplementary table summarizing experimental conditions, tracer types, dilution ratios, dip times, and measurement methods used during MagStick validation.